HHS Public Access

Author manuscript

Cancer Res. Author manuscript; available in PMC 2022 January 01.

Published in final edited form as:

Cancer Res. 2021 July 01; 81(13): 3717–3726. doi:10.1158/0008-5472.CAN-20-3626.

Nedd9 restrains autophagy to limit growth of early stage non-small cell lung cancer

Alexander Y. Deneka[1,2], **Meghan C. Kopp**[1,3], **Anna S. Nikonova**[1], **Anna V. Gaponova**[1], **Anna A. Kiseleva**[1,2], **Harvey H. Hensley**[1], **Douglas B. Flieder**[4], **Ilya G. Serebriiskii**[1,2], **Erica A. Golemis**[1,*]

[1]Program in Molecular Therapeutics, Fox Chase Cancer Center, Philadelphia, PA, 19111

[2]Kazan Federal University, 420000, Kazan, Russian Federation

[3]Cancer Biology, Drexel University College of Medicine, Philadelphia, PA 19129, USA

[4]Department of Pathology, Fox Chase Cancer Center, Philadelphia, PA, 19111

Abstract

Non-small cell lung cancer (NSCLC) is the most common cancer worldwide. With overall 5-year survival estimated at <17%, it is critical to identify factors that regulate NSCLC disease prognosis. NSCLC is commonly driven by mutations in *KRAS* and *TP53*, with activation of additional kinases such as SRC promoting tumor invasion. In this study, we investigated the role of NEDD9, a SRC activator and scaffolding protein, in NSCLC tumorigenesis. In an inducible model of NSCLC dependent on *Kras* mutation and *Trp53* loss (*KP* mice), deletion of *Nedd9* (*KPN* mice) led to the emergence of larger tumors characterized by accelerated rates of tumor growth and elevated proliferation. Orthotopic injection of *KP* and *KPN* tumors into the lungs of *Nedd9*-wildtype and -null mice indicated the effect of *Nedd9* loss was cell-autonomous. Tumors in *KPN* mice displayed reduced activation of SRC and AKT, indicating that activation of these pathways did not mediate enhanced growth of KPN tumors. NSCLC tumor growth has been shown to require active autophagy, a process dependent on activation of the kinases LKB1 and AMPK. *KPN* tumors contained high levels of active LKB1 and AMPK and increased autophagy compared to *KP* tumors. Treatment with the autophagy inhibitor chloroquine completely eliminated the growth advantage of KPN tumors. These data for the first time identify NEDD9 as a negative regulator of LKB1/AMPK-dependent autophagy during early NSCLC tumor growth.

Keywords

HEF1; AMPK; KRAS; LKB1; TP53; lung cancer

[*]corresponding author: Erica Golemis, Fox Chase Cancer Center, 333 Cottman Ave., Philadelphia, PA 19111, (215) 728-2860, Erica.Golemis@fccc.edu.

Disclosures: The authors declare no potential conflicts of interest.

Introduction.

Approximately 7% of individuals born in the United States will ultimately be diagnosed with lung cancer; in 2019, ~228,000 individuals were diagnosed as new cases and ~142,000 individuals died from this disease in the US alone (1). Non-small cell lung cancer (NSCLC), accounting for ~85% of lung cancer diagnoses, typically has a poor prognosis if tumors have disseminated from the primary site (2). Somatic activating mutations of *KRAS* accompanied by inactivating mutations of the tumor suppressor *TP53* are some of the most common oncogenic driver mutations in NSCLC, associated with resistance to some chemotherapies and targeted therapies (3,4). In addition to genomic changes, numerous signaling pathways are indirectly activated to support tumor progression. These include the SRC signaling cascade, which has been reported to enhance EGFR and KRAS effector activity and invasion (5,6), and the LKB1/AMPK signaling cascade, which fuels tumor growth by increasing autophagy (7,8).

NEDD9 (also known as HEF1 and Cas-L (9–11)) is a scaffolding protein that supports the activation of SRC and FAK to increase the pro-migratory and invasive signaling of solid tumors (9,12,13). In lung cancer, mutational loss of *LKB1* has been shown to induce NEDD9 transcription (14), with elevated NEDD9 levels supporting the increased metastasis of *LKB1*-null tumors (15), and likely contributing to the activation of SRC observed in these tumors (5). However, in at least 50% of NSCLC, *KRAS* activating mutations occur in the absence of *LKB1* mutations (16), and the role of *NEDD9* in tumorigenesis is not known.

To explore this issue, we used mouse models of NSCLC, crossing mice with a *Nedd9* null allele (17) to the inducible $Kras^{tm4Tyj/J}/Trp53^{tm1Brn/J}$ (*KP*) mouse model of lung adenocarcinoma, in which inhalation of adenovirus bearing Cre recombinase causes expression of an activating G12D allele of *Kras* (18) and deletes exons 2-10 of *Trp53*, resulting in a null allele (19). This work unexpectedly revealed that formation and growth of NSCLC tumors was significantly enhanced in the absence of Nedd9. Mechanistic investigations for the first time established that tumor formation in the absence of *Nedd9* activates Liver Kinase B1 (LKB1) and its effector AMP-activated protein kinase (AMPK). We further show that inhibition of autophagy completely reverses the growth advantage of *Nedd9*-deficient NSCLC, and that the consequences of Nedd9 deficiency are cell-autonomous, and distinct from its role in controlling SRC activation. Together, this work defines a previously unknown function for Nedd9 in regulation of autophagy.

Materials and Methods.

Mouse strains and drug treatment.

All experiments involving mice were approved by the Institutional Animal Care and Use Committee (IACUC) of Fox Chase Cancer Center. B6.129S/S4-$Kras^{tm4Tyj/J}$ mice (Jackson Laboratories #008179, Bar Harbor, ME, RRID:IMSR_GPT:T008179) were crossed to B6.129P2-$Trp53^{tm1Brn}$ mice (Jackson Laboratories #008462, Bar Harbor, ME, RRID:IMSR_GPT:T008462) to generate *KP* mice. These animals were crossed with mice bearing a null allele of *NEDD9* (17) ($Kras^{tm4Tyj/J}/Trp53^{tm1Brn/J}$;$Nedd9^{-/-}$, *KPN* mice), and tumor formation induced with inhalation of adenovirus bearing Cre at 9 weeks of age (20);

surviving mice were euthanized as 39 weeks of age. Dasatinib (#HY-10181, MedChemExpress, Monmouth Junction, NJ), or chloroquine (CQ, #C-6628, Sigma-Aldrich, St. Louis, MO, RRID:SCR_008988) were formulated in 5% dextrose vehicle, and administered at 10mg/kg and 50mg/kg respectively. Dosing with dasatinib or vehicle was performed by oral gavage daily, 5 days/week for 9 weeks, from 10 to 29 weeks of age. Dosing with CQ or vehicle was performed by daily intraperitoneal injection for 8 weeks, from 10 to 28 weeks of age. At 28-29 weeks of age, or earlier due to discernible distress, mice were euthanized by CO_2 inhalation.

For orthotopic xenografts, tumor material was manually excised from lungs of euthanized *KP* or *KPN* mice, dissected to 1-3 mm fragments, dissociated in collagenase/dispase-containing medium and homogenized using gentleMACS-C tubes (#130-093-237, Miltenyl Biotec, Auburn, CA). After counting using a Milipore automated cell counter (PHCC00000, EMD Millipore, Burlington, MA**,** RRID:SCR_008983), 500,000 cells were diluted in Matrigel and 100ul injected orthotopically into the right lungs of 9 week mice without Adeno-Cre activation of floxed *Kras* and *Trp53* alleles (functionally *Nedd9* wt (*kp)* or null (*kpN)* mice); mice were euthanized upon signs of distress.

Imaging by magnetic resonance imaging (MRI) and computed tomography (CT).

Mice were anesthetized with 2% isoflurane in O_2, and maintained in 0.5% isoflurane during MRI and CT scans. MRI scans were performed with a vertical bore 7-T magnet, Bruker DRX300 spectrometer, ParaVision 3.0.2 software (Bruker, Billerica, MA, RRID:SCR_001964), and a single tuned 1H cylindrical radiofrequency coil. Tumor volume was measured using Image J software (National Institutes of Health, Bethesda, MD, RRID:SCR_003070) to manually encircle tumor areas in multiple adjacent images. Volume estimations were calculated from image slice thickness x tumor areas, summed for each mouse. CT imaging was performed with a Sofie Biosciences CT/PET machine (G8 PET/CT, PerkinElmer/Sofie Biosciences, Culver City, CA, RRID:SCR_019155) using the standard protocol specified by the manufacturer. To calculate airspace volume, VivoQuant software (inviCRO, Boston, MA) was used. To identify the total area of air filled lung, areas with minimal contrast within a specific range, were automatically highlighted using the Connected Thresholding function. This setting was kept consistent for all analyzed mice. The airspace volume was calculated automatically in mm^3. Trachea and other artifacts were excluded manually.

Tissue preparation, histology, and quantitative analysis.

Lungs were fixed in 10% phosphate-buffered formaldehyde (formalin) for 24-48 hrs, paraffin-embedded, and sectioned at 5 μm thickness. Specimens were analyzed by hematoxylin and eosin (H&E) staining (Sigma-Aldrich, St. Louis, MO, RRID:SCR_008988) or by immunohistochemistry (IHC) using standard protocols. Slides were scanned using a Vectra Automated Quantitative Pathology Imaging System (Perkin Elmer, Waltham, MA, RRID:SCR_019155). All data were verified by a board-certified pathologist, using a standard grading protocol. Antibodies used for IHC or IF are listed in Supp Table 1. Expression levels of Ki-67, $ph^{T202/Y204}$Erk1/2, ph^{S428}Lkb1, and ph^{T172}Ampkα were quantified using inForm software (Perkin Elmer, Waltham, MA, RRID:SCR_019155). H-

score was calculated as the percentage of cells at each staining intensity level, using the formula: [1× (%cells 1+) + 2 × (%cells 2+) + 3 × (%cells 3+)] (21,22).

Immunofluorescence.

For some proteins, immunofluorescence was used to detect expression in FFPE tissue sections, using standard protocols. Antibodies used are listed in Supp Table 1. Slides were counterstained with Vectashield mounting medium with DAPI (4′, 6-diamidino-2-phenylindole) (H-1200, Vector Labs, Burlingame, CA, RRID:AB_2336790) solution to visualize DNA. Samples were imaged using an SP8 confocal system equipped with an oil-immersion 363 objective with numerical aperture 1.4 (Leica Microsystems, Buffalo Grove, IL) and LASAF (Leica Application Suite Advanced Fluorescence) software (Leica Microsystems, Buffalo Grove, IL, RRID:SCR_016555). Images were analyzed using Metamorph 7.6.5 software (Molecular Devices, Union City, CA, RRID:SCR_002368); integrated optical densities for each image were detected with the integrated morphometric analysis tool.

Cell culture.

The A549 (NCI-DTP Cat# A549, RRID:CVCL_0023), H460 (NCI-DTP Cat# NCI-H460, RRID:CVCL_0459), and H1299 (NCI-DTP Cat# NCI-H1299, RRID:CVCL_0060) human NSCLC cell lines were obtained from the American Type Culture Collection (ATCC), and their identity verified by STR profiling. Testing for Mycoplasma was negative and performed using PCR profiling. A549 cells were cultured in DMEM media, and H460, H1299 cells were cultured in RPMI-1640 media, in each case containing 10% fetal bovine serum (FBS), L-glutamine (L-glu) and penicillin/streptomycin (pen/strep). All cell lines were frozen upon delivery, thawed prior to experimental work and passaged for 3 weeks or less. For some experiments, cells were treated with vehicle (0.01% DMSO) or the SRC inhibitor dasatinib (#HY-10181, MedChemExpress, Monmouth Junction, NJ, 50nM for the A549 cell line, and 500nM for the H1299 cell line), the CaMKK inhibitor STO-609 (#HY-19805, MedChemExpress, Monmouth Junction, NJ, 500nM for all cell lines), or the FAK inhibitor PF-573228 (#HY-10461, MedChemExpress, Monmouth Junction, NJ, 500 nM for all cell lines) for 6 and 24 hrs prior to analysis.

Transient transfection.

NEDD9 Smartpool siRNA (with four pre-mixed siRNAs, cat# M-019466-02, target sequences 5’-AGGAACUGGCCUUUCGCAA-3’; 5’-CUACCAAAAUCAGGGAAUU-3’;5’-CCUCUGGACUGAUGCAGCA-3’; 5’-CCAAGAACAAGAGGUAUAU-3’) was purchased from Dharmacon (Lafayette, CO). Scrambled negative control siRNA (cat# AM4635) was purchased from Ambion (ThermoScientific, Waltham, MA, RRID:SCR_008452). NSCLC cells were plated in 6-well plates at 20% confluence, and transfected with siRNA at final concentrations of 30 nM using Lipofectamine RNAiMAX (#13778150, ThermoScientific, Waltham, MA, RRID:SCR_008452) transfection reagent according to the manufacturer’s instructions. Cells were harvested 48 hrs post-transfection for further analysis.

Western Blot Analysis.

Tumor tissues were lysed in T-PER (#78510, ThermoScientific, Waltham, MA, RRID:SCR_008452) or Cell-Lytic (#C-3228, Sigma-Aldrich, St. Louis, MO, RRID:SCR_008988) lysis buffers. Protein concentrations were established using the Pierce BCA Protein Assay Kit (#23225, Thermo Scientific, Waltham, MA, RRID:SCR_008452). Western blotting was performed using standard procedures, and blots developed using Luminata Western horseradish peroxidase (HRP) (Classico, WBLUC0500, Crescendo, WBLUR0500, and Forte, WBLUF0500, EMD Millipore, Burlington, MA, RRID:SCR_008983) and Immun-Star AP substrate (#1705018, Bio-Rad Laboratories, Hercules, CA, RRID:SCR_008426). Antibodies used are listed in Suppl Table S1. Quantification was done using NIH ImageJ Imaging Software (National Institutes of Health, Bethesda, MD, RRID:SCR_003070), and all values normalized to total Ponceau S (sc-301558, ChemCruz, Dallas, TX, RRID:SCR_008987) staining for each lane.

qRT-PCR analysis.

Total RNA was isolated from tumor tissues or cells using a Zymo Research Quick-RNA MicroPrep Kit (#R1050, Tustin, CA, RRID:SCR_008968) and tested for quality on a Bioanalyzer (Agilent Technologies, Santa Clara, CA, RRID:SCR_013575). RNA concentrations were determined with a NanoDrop spectrophotometer (Thermo Fisher Scientific, Waltham, MA, RRID:SCR_008452). RNA was reverse-transcribed using Moloney murine leukemia virus reverse transcriptase (#28025013, Ambion-Thermo Fisher Scientific, Waltham, MA, RRID:SCR_008452) and a mixture of anchored oligo-dT and random decamers (Integrated DNA Technologies, Coralville, IA, RRID:SCR_012186). Two reverse-transcription reactions were performed for each sample using either 100 or 25 ng of input RNA. Aliquots of the cDNA were used to measure the expression levels of the genes using the primers or the commercial assay (Thermo Fisher, RRID:SCR_008452) listed in Suppl Table S2, with expression of genes of interest normalized to that of the housekeeping gene 36B4. Assays were used in combination with Power SYBR Green master mix (Thermo Fisher, RRID:SCR_008452). All reactions were run on a 7900 HT sequence detection system (Applied Biosystems, Thermo Fisher Scientific Waltham, MA, RRID:SCR_008452). Cycling conditions were 95°C, 15 min, followed by 40 (two-step) cycles (95°C, 15 s; 60°C, 60 s). Ct (cycle threshold) values were converted to quantities (in arbitrary units) using a standard curve (four points, four-fold dilutions) established with a calibrator sample. For each sample, the values were averaged and standard deviation of data derived from two independent PCR experiments for each biological repeat.

Luminex assay.

For multiplex analysis, the Bio-Plex Pro Cell Signaling Akt Panel 8-Plex Assay kit (cat #LQ00006JK0K0RR, Bio-Rad Laboratories, Hercules, CA, RRID:SCR_008426) was used. Tissue samples were lysed using Cell-Lytic (#C-3228, Sigma-Aldrich, St. Louis, MO, RRID:SCR_008988) lysis buffer. Protein concentrations were established using the Pierce BCA Protein Assay Kit ((#23225, Thermo Scientific, Waltham, MA) and loaded in a 96-well plate containing magnetic beads for overnight incubation according to the manufacturer's protocols. The following day, protein signal was assessed using Bio-Plex 200

system (Bio-Rad Laboratories, Hercules, CA, RRID:SCR_008426). Results were processed using GraphPad Prism 6 (GraphPad Software, San Diego, CA, RRID:SCR_002798) software.

TCGA and GWAS analysis.

For analysis of publicly available datasets, the TCGA PanCancer datasets for NSCLC, bladder urothelial carcinoma, and hepatocellular carcinoma were accessed (January, 2021) and analyzed using tools available at cBioPortal for Cancer Genomics (http://www.cbioportal.org/) and Kaplan-Meier Plotter (http://kmplot.com). Genome-wide association study (GWAS) data for NEDD9 were identified from the GWAS catalog at the European Bioinformatics Institute (http://ebi.ac.uk/), the SNP catalog at NCBI (https://ncbi.nlm.nih.gov/), the COSMIC database (https://cancer.sanger.ac.uk), and the Cancer Genetics Catalog (http://cancer-genetics.org).

Statistical Analysis.

We used Wilcoxon Rank-sum two-tailed tests for pairwise comparisons, unless otherwise noted. Analyses including Kaplan-Meier analysis for survival were performed by using GraphPad Prism 6 (GraphPad Software, San Diego, CA, RRID:SCR_002798).

Results.

A *Nedd9* null genotype increases tumor burden and reduces survival in a conditional knockout *Kras/Trp53* mouse model for NSCLC.

To assess the consequence of constitutive absence of Nedd9 for NSCLC growth, we analyzed mice bearing wt or null alleles of *Nedd9* (17) crossed to the $Kras^{tm4Tyj/J}$ / $Trp53^{tm1Brn/J}$ mouse model (designated *KP* and *KPN* mice, respectively) (Fig 1A). Inhalation of adenovirus bearing Cre (Adeno-Cre) at postnatal week 9 activated *Kras* and inactivated *Trp53* in *KP* (n=33) and *KPN* (n=39) mice. Analysis of lungs by magnetic resonance imaging (MRI) (Fig 1B, C) at ~ 21, 25 and 29 weeks of age indicated significantly enhanced tumor growth in the *KPN* versus the *KP* cohort ($p<0.01$); similar results were made using CT (Figs S1A, S1B) to measure reduction in lung airspace volume. All mice were euthanized upon initial signs of distress, with all surviving mice euthanized at 39 weeks of age. Kaplan-Meier analysis (Fig 1D) indicated a significant reduction in survival of the *KPN* mice versus the *KP* mice (32 weeks versus 34 weeks of average survival; $p=0.0056$).

Histopathological assessment (Fig 1E) indicates the lungs of *KPN* mice had fewer distinguishable independent tumors (Fig 1F), but overall tumor area was greater (Fig 1G) and many individual tumors were larger (Fig 1H) than in *KP* mice, implying the reduction in numbers represented the merging of faster-growing tumors. *KPN* lung tumors also had a higher expression of the proliferation-associated Ki-67 protein (Figs 1I, S2A), and significantly increased phosphorylated Erk1/2 (Figs 1J, S2B), compatible with more rapid growth. 5/30 *KPN* mice had detectable tumor invasion of the heart, and 3/30 metastasis to other organs: however, no invasion or metastasis was detected among 23 *KP* mice (Fig 1E). KPN tumors were more likely than KP tumors to be detected at higher grade (stage 2 versus

stage 1, p<0.0001; Fig S2C). No differences were observed between KP and KPN tumors in level of apoptosis or tumor vascularization (Figs S2D, E).

The growth advantage of *KPN* tumors is tumor cell intrinsic, and independent of Src activation.

As Nedd9 is absent in all tissues of *KPN* mice, we evaluated whether loss of Nedd9 in NSCLC cancer cells versus in non-cancer tissue mediated the *KPN* tumor growth advantage. We orthotopically injected 0.5 x 10^6 primary *KPN* or *KP* tumor cells into the lungs of isogenic 9-week old *KP* or *KPN* mice but did not add Adeno-Cre to activate the floxed *Kras* and *Trp53* alleles (e.g., mice were functionally wt or *Nedd9 null*; recipient mice designated *kp* and *kpN*). Average survival of *kp* or *kpN* mice injected with *KPN* tumors was 20 days, in contrast to ~30 days average survival of mice injected with *KP* tumors (p<0.0003) (Fig 2A), and Erk1/2 phosphorylation was higher in *KPN* tumors (Fig 2B), indicating the growth phenotypes observed were largely cancer cell-intrinsic, rather than primarily a consequence of tumor microenvironment.

SRC kinase is the best established effector of NEDD9 (23), and elevated SRC activity is common and has growth-promoting effects in many tumors (24). To identify the molecular basis of the tumor-accelerating effect of Nedd9 loss, we first evaluated whether constitutive absence of *Nedd9* in *KPN* mice caused paradoxical, compensatory activation of Src. However, Western analysis of *KP* versus *KPN* mice indicated that absence of *Nedd9* strongly depressed Src activity (Fig 2C). We therefore evaluated whether inhibition of Src activity might promote tumor growth, or otherwise selectively influence tumor growth in *KP* versus *KPN* mice. For this purpose, we repeated tumorigenesis experiments in which *KP* and *KPN* mice were induced with Adeno-Cre at postnatal week 9, then treated either with vehicle (5% dextrose) or the SRC inhibitor dasatinib (10 mg/kg, 5 days a week) for 10 weeks, starting at age 19 weeks. MRI imaging was performed at 21, 25, and 29 weeks of age, after which mice were euthanized. By the experimental endpoint, dasatinib reduced the growth of *KP* tumors by 61% (tumor volume 6.34, versus 16.53 mm^3 in the vehicle treated group, p=0.21), but reduced the growth of *KPN* tumors by 83% (tumor volume 5.3, versus 32.6 mm^3 in the vehicle treated group, p=0.0027) (Fig 2D). Pathological assessment confirmed dasatinib removed the differential between tumor numbers in *KP* and *KPN* mice, and significantly reduced tumor area in *KPN* lungs (Fig 2E, F, Suppl Fig S2F, G), but did not affect vascularity or caspase staining (Supp Fig S2D, E).

These data indicated the growth advantage of *KPN* tumors did not arise from activation of the SRC pathway, causing us to consider alternative candidate signaling disruption. Activation of the mTOR/AKT/S6 signaling pathway is often associated with rapid tumor growth (25). However, using Luminex profiling of tumor lysates followed in some cases by Western validation, we found that the expression of ph^{S473}AKT, $ph^{S235/236}$S6, ph^{S2448}mTOR, and other proteins associated with more active protein synthesis was either comparable or lower in *KPN* versus *KP* tumors (Fig 2G). Further supporting the idea that the mTOR/S6K pathway was inhibited, *KPN* tumors expressed higher levels of ph^{S136}Bad, previously reported to be elevated as a consequence of mTOR pathway inhibition in lung cancer cells (26).

Constitutive Nedd9 loss promotes autophagic signaling *in vivo*.

Inhibition of the mTOR pathway is strongly associated with induction of autophagy, and growth of KRAS-dependent NSCLCs depends on efficient autophagy (8,27,28). In autophagy, increased LKB1 activation promotes activation of AMPK, triggering signaling cascades (Fig 3A) that results in activation of autophagic effectors, but inhibition of some mTOR effectors (29,30). Loss of *Lkb1* induces *Nedd9*, in a process that promotes metastasis (14). Given negative feedback loops are common elements of cell signaling networks (31), we considered the possibility that loss of *Nedd9* during tumorigenesis might reciprocally induce Lkb1.

Specific examination of tumor lysates from 8 *KPN* versus 8 *KP* mice by Western analysis indicated that activation of Lkb1 (ph^{S428}Lkb1) was very strongly increased in *KPN* compared to *KP* tumors, associated with parallel increase in Ampk activation (ph^{T172}Ampk) (Fig 3B). Strikingly, the activation of Lkb1 occurred in the context of significant downregulation of total Lkb1 in *KPN* tumors (Fig 3B). Comparison of steady state mRNA expression of *Lkb1* and *Ampk* from *KP* versus *KPN* tumors (Fig 3C) indicated comparable levels of expression in both genotypes, implying a post-transcriptional control mechanism. In accord with this interpretation, transient siRNA depletion of NEDD9 in two human NSCLC cell lines had no effect on *LKB1* or *AMPK* mRNA expression (Fig 3D), but elevated LKB1 and AMPK activation; although the magnitude of the effect was less, these data paralleled *in vivo* results (Fig 3E). Investigating candidate effectors that might mediate NEDD9 action, we determined that inhibition of neither FAK nor CaMKK (reported as an activator of AMPK, (29)) affected LKB1 mRNA or protein expression, or enhanced LKB1 phosphorylation, whereas inhibition of SRC elevated LKB1 phosphorylation at least transiently (Supp Fig S3A, B).

Reduced mTORC2 signaling and elevated autophagic signaling in KPN versus KP tumors.

We investigated activation of AMPK-dependent signaling pathways in *KPN* versus *KP* tumors (Fig 4). *KPN* tumors had significantly elevated AMPK-dependent phosphorylation of the autophagic effector Ulk1 (ph^{S555}Ulk1; versus no significant change in mTORC1-phosphorylated ph^{S757}Ulk1), and total expression of LC3B-I, LC3B-II, Atg5, and p62 (Fig 4A). Immunofluorescence analysis of tumor sections indicated more areas of tumor containing LC3B- and Atg5-positive autophagosomes in the lung tumors of *KPN* versus *KP* mice (Figs 4B, C, Supp Fig S4A). To explore whether altered signaling by the Nedd9-interacting Src protein contributed to the elevated autophagy observed in *KPN* tumors, we also analyzed vehicle- versus dasatinib-treated *KP* and *KPN* tumors. Notably, Src inhibition eliminated the elevated levels of ph^{S428}Lkb1 and ph^{T172}Ampkα in *KPN* tumors (Fig 4D, Supp Fig S4B). Together, these data indicated that absence of Nedd9 during tumorigenesis stimulated autophagy through induction of Lkb1 activity, and that inhibition of Src kinase influenced Nedd9 control of Lkb1 activity.

In parallel, we observed that overall levels of the mTOR protein, and autophosphorylated active ph^{S2481}mTOR were reduced relative to *KP* tumors (Fig 4E). Phosphorylation of substrates of mTORC1 (ph^{S371}S6K and $ph^{S235/236}$S6) did not significantly differ between the two genotypes (Fig 4F). However, activating phosphorylation of the mTORC2 substrate

S^{473}AKT was considerably reduced in KPN tumors, as was AKT-dependent inhibitory phosphorylation of TSC2 (ph^{S939}TSC2, (32)) (Fig 4G), implying feedback downregulation of the mTORC2 signaling pathway.

Inhibition of autophagy eliminates the growth advantage of *KPN* tumors.

To directly test whether the greater growth of *KPN* tumors required elevated autophagy, we initiated tumor growth in 9 week old *KP* and *KPN* mice as described above, and after 10 weeks dosed mice with vehicle or the autophagy inhibitor chloroquine (CQ) at 50 mg/kg daily for 8 weeks. CT evaluation of airspace volume indicated that by 6 weeks after the beginning of drug treatment, the loss of airspace in CQ-treated *KPN* mice was less than in vehicle-treated *KPN* mice, and comparable to that seen in *KP* mice treated with either vehicle or CQ; these differences were statistically significant after 8 weeks (Fig 5A). For both *KP* and *KPN* mice, CQ significantly reduced tumor area (Fig 5B); notably, CQ completely eliminated the size differential between *KPN* and *KP* tumors. Notably, CQ-treated *KPN* mice developed none of the very large tumors observed in vehicle-treated *KPN* mice (Fig 5C).

Mechanistically, CQ acts by blocking autophagosome fusion with lysosomes, blocking the scavenging of degraded proteins; this downstream blockade typically elevates expression of proteins that promote autophagy and accumulation of autophagosome cargo proteins, including LC3B but not p62 (Fig 3A and (33)). Using quantitative IHC analysis of tumors, we confirmed CQ treatment highly elevated ph^{S428}Lkb1 and ph^{T172}AMPKα expression in both KP and KPN tumors, eliminating the differential in which these proteins are more highly expressed in the KPN tumor genotype (Figs 5D, E, Supp Fig S4B). In concord with blockade of autophagosome fusion, the level of Atg5- and LC3B-positive autophagosomes was highly elevated in CQ-treated *KP* and *KPN* NSCLCs (Fig 5F). Notably, although CQ did not affect tumor vascularity, apoptosis was markedly elevated in KPN versus KP tumors in CQ-treated mice (Supp Fig S2D, E), in accord with the marked effect of CQ in inhibiting the growth of KPN tumors. These results confirmed the importance of activation of autophagy as a primary mechanism by which absence of *Nedd9* promoted tumorigenesis.

NEDD9 expression and survival in human lung cancer.

Previous studies have documented increases in NEDD9 expression during progression of various tumors and linked higher expression of NEDD9 in metastatic tumors to poor survival outcomes (34). In this study, we instead found reducing NEDD9 expression leads to more rapid early tumor growth. To gain insight into these distinct patterns, we analyzed public resources reporting GWAS, mutation, and expression patterns for NEDD9 in humans (Supp Fig S5, Supp Table S3). No germline variants affecting NEDD9 coding sequences have been reported. Some intronic variants have been associated with risk for prostate, small cell lung cancer, and other cancers have been reported. For prostate cancer, the effect of the variant (rs4713266, enriched in individuals of African descent) is to increase NEDD9 expression (35); for other variants, the effect on protein expression is not known. NEDD9 is rarely mutated, amplified, or deleted in lung adenocarcinomas (Supp Fig S5A). As lung tumors grow, the majority of tumors retain NEDD9 mRNA expression within a narrow range; however, a sub-population of tumors has significant elevation of NEDD9 mRNA

(Supp Fig S5B, S6). Notably, if we compare T1, T2, and T3 tumors, which are distinguished by size of the primary tumor, those with the lowest quartile of NEDD9 expression are associated with worse outcomes than those with the highest quartile of NEDD9 expression in T1 tumors. Interestingly, these differences are reduced in T2 tumors, and further reduced in T3 tumors. If only non-invasive tumors are considered, the degree of risk associated with is actually reverses in T3 tumors, compatible with the hypothesis that NEDD9 is tumor-suppressive at early stages of tumor growth, and tumor-promoting at later stages. Similar patterns are observed in evaluating tumors by stage not only for lung, but also for bladder and liver cancers (Supp Fig S6).

Discussion.

In this study, we demonstrate that Kras/Trp53-dependent NSCLC tumorigenesis in the absence of Nedd9 results in a more aggressive disease. Based on orthotopic transplantation experiments, we show that this reflects a tumor cell intrinsic phenotype, rather than an effect of tumor microenvironment. This aggressive disease reflects post-transcriptional induction of Lkb1/Ampk signaling that promotes autophagy in Nedd9-deficient NSCLC cancer cells, and is the first report of a role for Nedd9 in regulation of Lkb1 or autophagy.

These were unexpected results. Typically, studies of NEDD9 depletion or deletion in established cancer models has focused on how this depletion limits migration (36). These phenotypes derive from loss of NEDD9 function as a scaffold and signaling intermediate for plasma membrane-associated integrins, chemokine receptors, receptor tyrosine kinases (10), and for pro-invasive TGF signaling (37), based on NEDD9 regulation of SRC, FAK, and associated effectors (38–41). Previous extensive studies have indicated that a *Nedd9* null genotype delays and reduced overall tumorigenesis in two independent mouse models for mammary cancer (38,42). Further, in a genetic $Kras^{G12D};Lkb1^{L/L}$ mouse model of NSCLC lung cancer model, shRNA reduction of Nedd9 in 8 week old mice led to no significant change in tumor area or number when mice were assessed 21 weeks later (15).

We propose several reasons for the very different results seen in this study. First, the physiological $Kras^{tm4Tyj/J}/Trp53^{tm1Brn/J}$ (KP) mouse model used in this study grows more aggressively than other tumor models in which Nedd9 loss was previously assessed, and as in human NSCLC, this rapid growth depends on autophagy to support a more active metabolism (8,28). Second, the single prior study of Nedd9 loss in lung cancer formation was performed in a model without intact Lkb1, which would have eliminated the pro-autophagic signaling we identify here; indeed, the contrasting results in that study support our interpretation of the important role for Lkb1 in induction of autophagy by Nedd9 loss. Loss of LKB1 has previously been shown to induce NEDD9 expression (15). Based on our data, a reciprocal relationship pertains, in which loss or knockdown of NEDD9 decreases protein expression of Lkb1, but leads to a more active kinase, positioning NEDD9 to influence autophagy under conditions requiring rapid growth (43).

In this context, it is notable that we observe the specific signaling consequences of Nedd9 loss primarily in the emergence of a set of fast-growing, larger tumors that are specifically vulnerable to apoptosis upon administration of cloroquine. This vulnerability may in part be

related to downregulation of mTorc2 phosphorylation of Akt, reducing survival signaling in KPN tumors. In addition, prior studies have noted that LKB1 activity and stabilized by RAS-dependent polyubiquitination by S-phase kinase-associated protein 2 (SKP2), -Cullin-F-box (SCF) ubiquitin ligase complex, which promotes interaction with a complex containing STE20-related kinase adaptor (STRAD) and mouse protein 25 (MO25, also known as CAB39) (44). In addition, sumoylation of LKB1 on K178 as a result of energy stress has also been shown to promote its activation of AMPK and downstreatm effectors (45). The specific mechanism by which Lkb1 expression responds to loss of Nedd9 requires further investigation.

Another factor that may contribute to differences between this study and earlier works is the possibility that NEDD9 functions differently during early versus later stages of tumor growth. A model for such variable function is TGFβ, which is tumor-suppressive prior to cell transformation, but tumor-promoting for transformed cells (46). The changing correlation between low NEDD9 mRNA expression and survival outcomes based on analysis of TCGA data (Supp Fig S5) would be in accord with such an interpretation. Notably, while a prior study of NEDD9 expression and prognosis in human lung tumor specimens identified a correlation between NEDD9 expression and poor prognosis, the specimens analyzed were biased towards advanced tumors (47). Intriguingly, NEDD9 function has previously been shown to linked to activation of TGFβ signaling, based on a direct interaction between NEDD9 and the TGF effector SMAD3 (48). Investigation of a potential reversal of NEDD9 function in early versus advanced tumors merits further investigation. Such a NEDD9 growth-inhibitory function in early tumors would be tissue specific, and may be linked to the specific requirement of lung tumors for autophagic signaling.

Mechanistically, Nedd9 is one of a group of CAS-family proteins that interact with Src to enhance phosphorylation of various downstream effectors, most of which have been studied in the context of control of metastasis (10,49). The Src inhibitor dasatinib reduces *Kras/Trp53* mutation-associated NSCLC tumor growth in clinical studies (50). Strikingly, although Src activity is decreased in fast-growing KPN tumors expressing higher levels of ph^{S428}Lkb1 versus slower-growing KP tumors, dasatinib treatment both decreases ph^{S428}Lkb1 expression and further decreases tumor growth, regardless of genotype. These observations, are compatible with a model in which Nedd9 deficiency promotes rapid tumor growth by inducing Lkb1/Ampk signaling and autophagy through a mechanism that requires at least minimal levels of Src kinase activity in cells.

In retrospect, the early appearance of studies focusing on the upregulation of NEDD9 as tumors become invasive and metastatic (10) concentrated subsequent research efforts on elucidating the frequency and consequences of elevated NEDD9 expression in tumor progression. Our work for the first time suggests that Nedd9 has a role in limiting autophagy at early stages of tumor growth, and that this must be overcome by progressive changes in oncogenic signaling networks before NSCLC cells tolerate NEDD9 upregulation. We note, our studies have been performed in a KRAS/TP53-dependent cancer model. Whether NEDD9 will be have a similar role in other subtypes of NSCLC, including in genetically

distinct tumors dependent on mutations in EGFR, ALK, or other oncogenes (51), which have significant differences in signaling dependencies, remains to be assessed.

Given the interest in therapeutically targeting autophagy (e.g. (52)), and given NEDD9 expression varies significantly among tumors, this protein merits investigation as a potential biomarker for response to autophagic inhibitors, at least in NSCLC dependent on mutations in *KRAS* and with intact *LKB1*. In addition, the results have potential implications for other therapies of value for NSCLC, including promising agents such as the immune checkpoint inhibitor (ICI) nivolumab, which targets PD-1/PD-L1 interactions. Of particular interest, mutational inactivation of *LKB1* is associated with an “immune cold” environment, and failure to respond to ICI inhibitors in KRAS-mutated human NSCLC (53). By defining Nedd9 as a regulator of Lkb1 activation, our data suggest that Nedd9 expression may also be a potential biomarker for in vivo response to ICIs, and that inhibition of Nedd9 may be a means of sensitizing NSCLCs to these agents.

Supplementary Material

Refer to Web version on PubMed Central for supplementary material.

Acknowledgments.

We would like to thank Dr. Essel Al-Saleem and Dr. Earl Pape for their assistance conducting the pathological grading analysis presented in Figure S2, Dr. Margret Einarson for help with Luminex analysis; and Dr. Emmanuelle Nicolas for help with RT-PCR. We acknowledge the Fox Chase Cancer Center Facilities for Laboratory Animals, Histopathology, Biological Imaging, Genomics, and Translational Research.

Financial support:

The authors and study were supported by DOD W81X-14-01-0135, and support from the William Wikoff Smith Charitable Trust and S10 OD021754 (to EAG); by NIH T32 CA009035 (to AN); by a William J. Avery Postdoctoral Fellowship from Fox Chase Cancer Center and a Russian Science Foundation project 18-75-00104 (to AD); by the Russian Government Program for Competitive Growth of Kazan Federal University (to AK and AD); and by the NCI Core Grant P30 CA006927 (to Fox Chase Cancer Center).

References.

1. Miller KD, Nogueira L, Mariotto AB, Rowland JH, Yabroff KR, Alfano CM, et al. Cancer treatment and survivorship statistics, 2019. CA Cancer J Clin 2019;69:363–85 [PubMed: 31184787]
2. Siegel RL, Miller KD, Jemal A. Cancer statistics, 2020. CA Cancer J Clin 2020;70:7–30 [PubMed: 31912902]
3. Karachaliou N, Mayo C, Costa C, Magri I, Gimenez-Capitan A, Molina-Vila MA, et al. KRAS mutations in lung cancer. Clin Lung Cancer 2013;14:205–14 [PubMed: 23122493]
4. Takahashi T, Nau MM, Chiba I, Birrer MJ, Rosenberg RK, Vinocour M, et al. p53: a frequent target for genetic abnormalities in lung cancer. Science 1989;246:491–4 [PubMed: 2554494]
5. Carretero J, Shimamura T, Rikova K, Jackson AL, Wilkerson MD, Borgman CL, et al. Integrative genomic and proteomic analyses identify targets for Lkb1-deficient metastatic lung tumors. Cancer Cell 2010;17:547–59 [PubMed: 20541700]
6. Tice DA, Biscardi JS, Nickles AL, Parsons SJ. Mechanism of biological synergy between cellular Src and epidermal growth factor receptor. Proc Natl Acad Sci U S A 1999;96:1415–20 [PubMed: 9990038]
7. Mowers EE, Sharifi MN, Macleod KF. Autophagy in cancer metastasis. Oncogene 2017;36:1619–30 [PubMed: 27593926]

8. Karsli-Uzunbas G, Guo JY, Price S, Teng X, Laddha SV, Khor S, et al. Autophagy is required for glucose homeostasis and lung tumor maintenance. Cancer Discov 2014;4:914–27 [PubMed: 24875857]
9. Law SF, Estojak J, Wang B, Mysliwiec T, Kruh GD, Golemis EA. Human Enhancer of Filamentation 1 (HEF1), a novel p130Cas-like docking protein, associates with FAK, and induces pseudohyphal growth in yeast. Mol Cell Biol 1996;16:3327–37 [PubMed: 8668148]
10. Shagisultanova E, Gaponova AV, Gabbasov R, Nicolas E, Golemis EA. Preclinical and clinical studies of the NEDD9 scaffold protein in cancer and other diseases. Gene 2015
11. Minegishi M, Tachibana K, Sato T, Iwata S, Nojima Y, Morimoto C. Structure and function of Cas-L, a 105-kD Crk-associated substrate-related protein that is involved in beta-1 integrin-mediated signaling in lymphocytes. J Exp Med 1996;184:1365–75 [PubMed: 8879209]
12. van Seventer GA, Salman HJ, Law SF, O'Neill GM, Mullen MM, Franz AA, et al. Focal adhesion kinase regulates beta1 integrin dependent migration through an HEF1 effector pathway. Eur J Imm 2001;31:1417–27
13. Bui LC, Tomkiewicz C, Chevallier A, Pierre S, Bats AS, Mota S, et al. Nedd9/Hef1/Cas-L mediates the effects of environmental pollutants on cell migration and plasticity. Oncogene 2009;28:3642–51 [PubMed: 19648964]
14. Ji H, Ramsey MR, Hayes DN, Fan C, McNamara K, Kozlowski P, et al. LKB1 modulates lung cancer differentiation and metastasis. Nature 2007;448:807–10 [PubMed: 17676035]
15. Feng Y, Wang Y, Wang Z, Fang Z, Li F, Gao Y, et al. The CRTC1-NEDD9 signaling axis mediates lung cancer progression caused by LKB1 loss. Cancer Res 2012;72:6502–11 [PubMed: 23074285]
16. Sanchez-Cespedes M, Parrella P, Esteller M, Nomoto S, Trink B, Engles JM, et al. Inactivation of LKB1/STK11 is a common event in adenocarcinomas of the lung. Cancer Res 2002;62:3659–62 [PubMed: 12097271]
17. Seo S, Asai T, Saito T, Suzuki T, Morishita Y, Nakamoto T, et al. Crk-associated substrate lymphocyte type is required for lymphocyte trafficking and marginal zone B cell maintenance. J Immunol 2005;175:3492–501 [PubMed: 16148091]
18. Jackson EL, Willis N, Mercer K, Bronson RT, Crowley D, Montoya R, et al. Analysis of lung tumor initiation and progression using conditional expression of oncogenic K-ras. Genes Dev 2001;15:3243–8 [PubMed: 11751630]
19. Marino S, Vooijs M, van Der Gulden H, Jonkers J, Berns A. Induction of medulloblastomas in p53-null mutant mice by somatic inactivation of Rb in the external granular layer cells of the cerebellum. Genes Dev 2000;14:994–1004 [PubMed: 10783170]
20. Jackson EL, Olive KP, Tuveson DA, Bronson R, Crowley D, Brown M, et al. The differential effects of mutant p53 alleles on advanced murine lung cancer. Cancer Res 2005;65:10280–8 [PubMed: 16288016]
21. Saeed AI, Sharov V, White J, Li J, Liang W, Bhagabati N, et al. TM4: a free, open-source system for microarray data management and analysis. Biotechniques 2003;34:374–8 [PubMed: 12613259]
22. John T, Liu G, Tsao MS. Overview of molecular testing in non-small-cell lung cancer: mutational analysis, gene copy number, protein expression and other biomarkers of EGFR for the prediction of response to tyrosine kinase inhibitors. Oncogene 2009;28 Suppl 1:S14–23 [PubMed: 19680292]
23. O'Neill GM, Fashena SJ, Golemis EA. Integrin signaling: a new Cas(t) of characters enters the stage. Trends Cell Biol 2000;10:111–9 [PubMed: 10675905]
24. Ishizawar R, Parsons SJ. c-Src and cooperating partners in human cancer. Cancer Cell 2004;6:209–14 [PubMed: 15380511]
25. Papadimitrakopoulou V Development of PI3K/AKT/mTOR pathway inhibitors and their application in personalized therapy for non-small-cell lung cancer. J Thorac Oncol 2012;7:1315–26 [PubMed: 22648207]
26. Liu Y, Sun SY, Owonikoko TK, Sica GL, Curran WJ, Khuri FR, et al. Rapamycin induces Bad phosphorylation in association with its resistance to human lung cancer cells. Mol Cancer Ther 2012;11:45–56 [PubMed: 22057915]
27. Bhanot H, Reddy MM, Nonami A, Weisberg EL, Bonal D, Kirschmeier PT, et al. Pathological glycogenesis through glycogen synthase 1 and suppression of excessive AMP kinase activity in myeloid leukemia cells. Leukemia 2015;29:1555–63 [PubMed: 25703587]

28. Guo JY, White E. Autophagy is required for mitochondrial function, lipid metabolism, growth, and fate of KRAS(G12D)-driven lung tumors. Autophagy 2013;9:1636–8 [PubMed: 23959381]
29. Hardie DG. AMPK--sensing energy while talking to other signaling pathways. Cell Metab 2014;20:939–52 [PubMed: 25448702]
30. Lin SC, Hardie DG. AMPK: Sensing Glucose as well as Cellular Energy Status. Cell Metab 2018;27:299–313 [PubMed: 29153408]
31. Chandarlapaty S Negative feedback and adaptive resistance to the targeted therapy of cancer. Cancer Discov 2012;2:311–9 [PubMed: 22576208]
32. Cai SL, Tee AR, Short JD, Bergeron JM, Kim J, Shen J, et al. Activity of TSC2 is inhibited by AKT-mediated phosphorylation and membrane partitioning. J Cell Biol 2006;173:279–89 [PubMed: 16636147]
33. Klionsky DJ, Abdelmohsen K, Abe A, Abedin MJ, Abeliovich H, Acevedo Arozena A, et al. Guidelines for the use and interpretation of assays for monitoring autophagy (3rd edition). Autophagy 2016;12:1–222 [PubMed: 26799652]
34. Shagisultanova E, Gaponova AV, Gabbasov R, Nicolas E, Golemis EA. Preclinical and clinical studies of the NEDD9 scaffold protein in cancer and other diseases. Gene 2015;567:1–11 [PubMed: 25967390]
35. Han D, Owiredu JN, Healy BM, Li M, Labaf M, Steinfeld JS, et al. Susceptibility-associated genetic variation in NEDD9 contributes to prostate cancer initiation and progression. Cancer Res 2021
36. O'Neill GM, Seo S, Serebriiskii IG, Lessin SR, Golemis EA. A new central scaffold for metastasis: parsing HEF1/Cas-L/NEDD9. Cancer Res 2007;67:8975–9 [PubMed: 17908996]
37. Liu X, Elia AEH, Law SF, Golemis EA, Farley J, Wang T. A novel ability of Smad3 to regulate proteasomal degradation of a Cas family member, HEF1. EMBO J 2000;19:6759–69 [PubMed: 11118211]
38. Izumchenko E, Singh MK, Plotnikova OV, Tikhmyanova N, Little JL, Serebriiskii IG, et al. NEDD9 promotes oncogenic signaling in mammary tumor development. Cancer Res 2009;69:7198–206 [PubMed: 19738060]
39. Sanz-Moreno V, Gadea G, Ahn J, Paterson H, Marra P, Pinner S, et al. Rac activation and inactivation control plasticity of tumor cell movement. Cell 2008;135:510–23 [PubMed: 18984162]
40. Tikhmyanova N, Golemis EA. NEDD9 and BCAR1 negatively regulate E-cadherin membrane localization, and promote E-cadherin degradation. PLoS One 2011;6:e22102 [PubMed: 21765937]
41. Pugacheva EN, Golemis EA. HEF1-aurora A interactions: points of dialog between the cell cycle and cell attachment signaling networks. Cell Cycle 2006;5:384–91 [PubMed: 16479169]
42. Little JL, Serzhanova V, Izumchenko E, Egleston BL, Parise E, Klein-Szanto AJ, et al. A requirement for Nedd9 in luminal progenitor cells prior to mammary tumorigenesis in MMTV-HER2/ErbB2 mice. Oncogene 2013
43. Herzig S, Shaw RJ. AMPK: guardian of metabolism and mitochondrial homeostasis. Nat Rev Mol Cell Biol 2018;19:121–35 [PubMed: 28974774]
44. Lee SW, Li CF, Jin G, Cai Z, Han F, Chan CH, et al. Skp2-dependent ubiquitination and activation of LKB1 is essential for cancer cell survival under energy stress. Mol Cell 2015;57:1022–33 [PubMed: 25728766]
45. Ritho J, Arold ST, Yeh ET. A Critical SUMO1 Modification of LKB1 Regulates AMPK Activity during Energy Stress. Cell reports 2015;12:734–42 [PubMed: 26212320]
46. Huang JJ, Blobe GC. Dichotomous roles of TGF-beta in human cancer. Biochem Soc Trans 2016;44:1441–54 [PubMed: 27911726]
47. Miao Y, Li AL, Wang L, Fan CF, Zhang XP, Xu HT, et al. Overexpression of NEDD9 is associated with altered expression of E-Cadherin, beta-Catenin and N-Cadherin and predictive of poor prognosis in non-small cell lung cancer. Pathol Oncol Res 2013;19:281–6 [PubMed: 23086683]
48. Samokhin AO, Stephens T, Wertheim BM, Wang RS, Vargas SO, Yung LM, et al. NEDD9 targets COL3A1 to promote endothelial fibrosis and pulmonary arterial hypertension. Sci Transl Med 2018;10

49. Deneka A, Korobeynikov V, Golemis EA. Embryonal Fyn-associated substrate (EFS) and CASS4: The lesser-known CAS protein family members. Gene 2015;570:25–35 [PubMed: 26119091]

50. Johnson FM, Bekele BN, Feng L, Wistuba I, Tang XM, Tran HT, et al. Phase II study of dasatinib in patients with advanced non-small-cell lung cancer. J Clin Oncol 2010;28:4609–15 [PubMed: 20855820]

51. Rotow J, Bivona TG. Understanding and targeting resistance mechanisms in NSCLC. Nat Rev Cancer 2017;17:637–58 [PubMed: 29068003]

52. Guo JY, White E. Autophagy, Metabolism, and Cancer. Cold Spring Harb Symp Quant Biol 2016;81:73–8 [PubMed: 28209717]

53. Skoulidis F, Goldberg ME, Greenawalt DM, Hellmann MD, Awad MM, Gainor JF, et al. STK11/LKB1 Mutations and PD-1 Inhibitor Resistance in KRAS-Mutant Lung Adenocarcinoma. Cancer Discov 2018;8:822–35 [PubMed: 29773717]

Significance:

This study demonstrates a novel role for the scaffolding protein NEDD9 in regulating LKB1-AMPK signaling in early stage non-small cell lung cancer, suppressing autophagy and tumor growth.

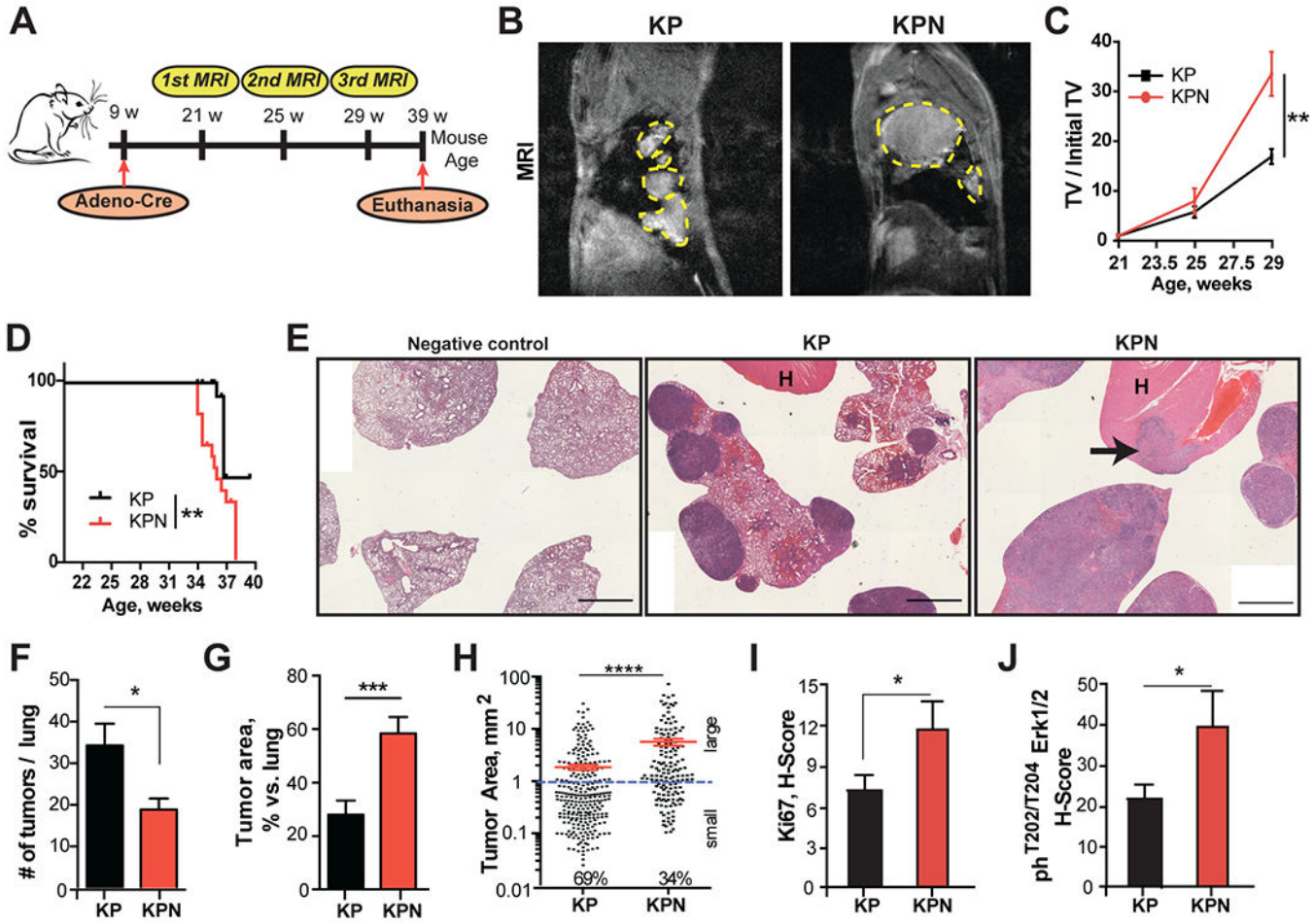

Figure 1. Comparison of NSCLC tumor formation in KP and KPN mice.

A. Outline of experimental design. Adenoviral activation of oncogenic *Kras G12D* and inactivation of *Trp53* was induced in 9 week old mice by introduction of 2.5^{e6} particles of adenovirus bearing Cre recombinase (UIowa-4, University of Iowa Viral Vector Core, Iowa City, IA) in 75 μl MEM media with 0.01M $CaCl_2$ into the trachea by normal inhalation in anesthetized mice, using standard procedures (20). Lung tumor formation was confirmed 12 weeks after activation and monitored by MRI and CT micro-imaging. **B, C**. Representative MRI images (29 weeks) (**B**) and quantitation (**C**) of NSCLC tumor volume (TV) in *KP* and *KPN* mice. Yellow dashed lines highlight tumors within lungs. **D**. Kaplan-Meier analysis comparing survival of *KPN* mice versus *KP* mice. **E**. Hematoxylin and eosin (H&E) stained lung and heart (H) tissue. Arrow indicates metastasis to heart. Scale bar = 500 um. **F-J**. Quantification of tumor number (**F**), tumor area (**G**), size of individual tumors (% indicates tumors with area < $1mm^2$) (**H**), H-score for Ki-67 (**I**), and H-score for phosphorylated $ph^{T202/Y204}Erk1/2$ (**J**), from *KP* versus *KPN* lungs. For panels **E-J**, following H&E or antibody staining, Vectra specific protocols and algorithms were used for the identification of tumor cells versus stromal tissue, with quantification of size and staining intensity based on use of Image J software (National Institutes of Health, Bethesda, MD). Based on Wilcoxon Rank-sum two-tailed tests, *, p<0.05, **, p<0.01, ***, p<0.001, ****, p<0.0001 for all graphs.

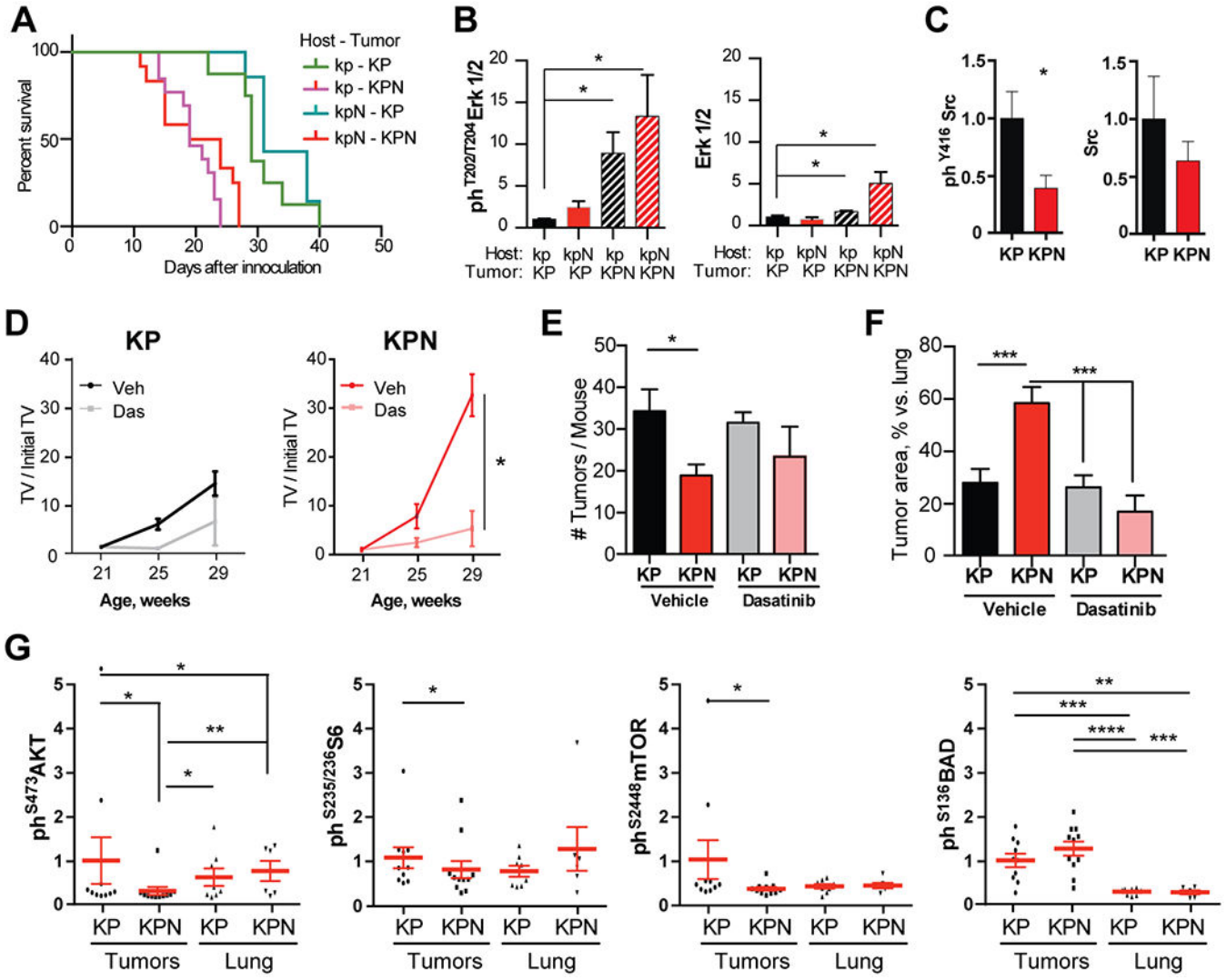

Figure 2. Elevated growth of KPN tumors is cell autonomous, and requires Src activity.

A. Kaplan-Meier analysis, comparing survival of *KP* and *KPN* host mice after orthotopic implantation of *KP* and *KPN* cancer cells from dissected tumors. *kp-KP* versus *kp-KPN*, p=0.0001; *kp-KP* versus *kpn-KP*, p=0.2602; *kp-KP* versus *kpn-KPN*, p=0.0003; *kp-KPN* versus *kpn-KPN*, p=0.1278. **B, C.** Quantitation of expression of indicated proteins in tumors from orthotopic injection experiments h. All values shown for Western blot quantitation are normalized to Ponceau S. Wilcoxon Rank-sum two-tailed tests; *, p<0.05, **, p<0.01, ***, p<0.001 versus control. **D.** Quantitation of increase in tumor volume (TV) over starting TV as established by MRI in *KP* and *KPN* mice treated with vehicle or dasatinib. **E-F.** Quantitation of number (**E**) and total area (**F**) of tumors in lungs of *KP* and *KPN* mice treated with vehicle or dasatinib, based on H&E analysis. **G**. Quantification from Luminex analysis of lysates prepared from dissected tumors or adjacent lung tissue for indicated analytes. *, p<0.05, **, p<0.01, ***, p<0.001, ****, p<0.0001 for all graphs.

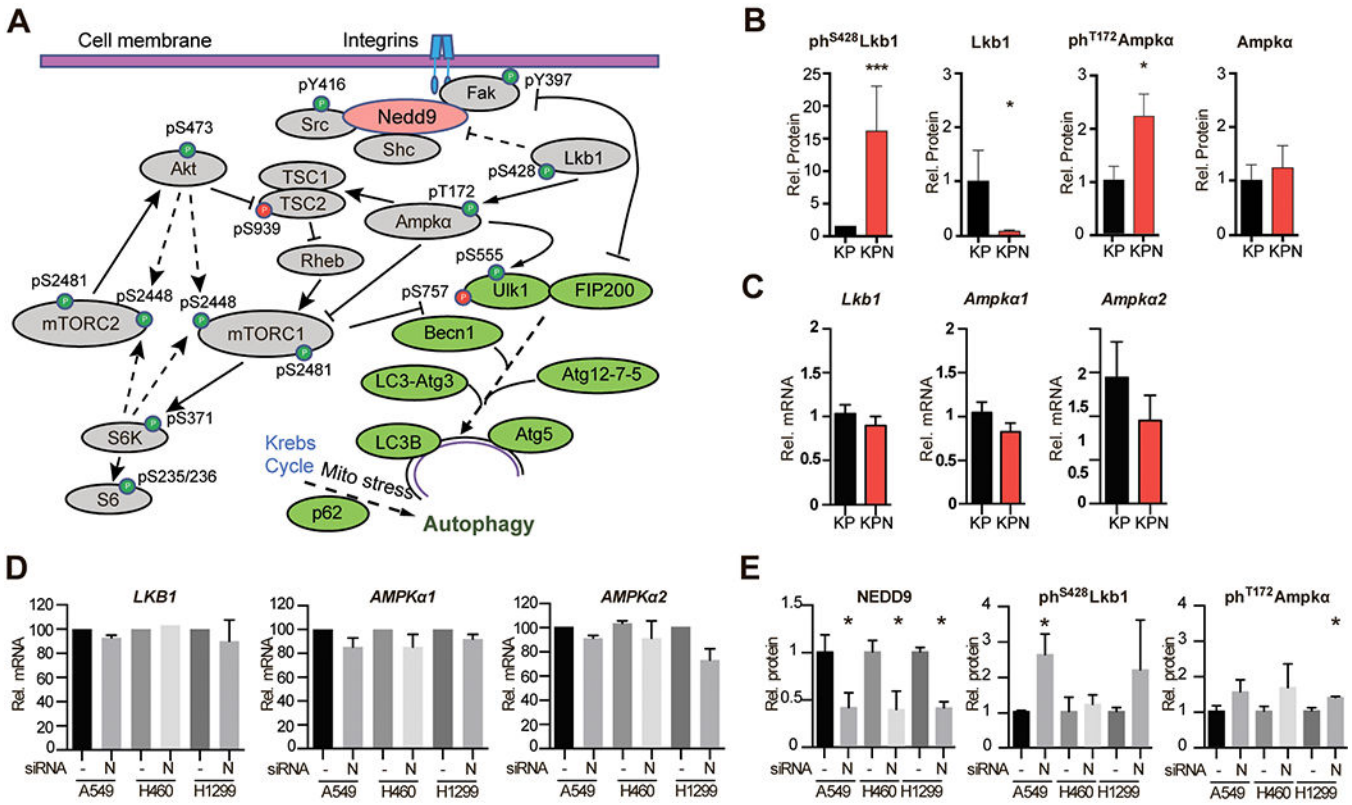

Figure 3. NEDD9 control of LKB1 activity.

A. Schematic of autophagic signaling pathway. **B.** Expression of phosphorylated Lkb1 and Ampk quantified from Western blots of *KP* and *KPN* tumor lysates. **C.** Expression of total mRNA for *Lkb1* (gene symbol, *Stk11*) and *Ampk* (two isoforms, *Prkaa1* and *Prkaa2*) quantified from RT-PCR of *KP* and *KPN* tumor lysates. **D, E.** mRNA (**D**) and protein (**E**) expression for NEDD9, LKB1, and AMPK in human NSCLC cell lines, following siRNA depletion of NEDD9 (“N”), versus treatment with control scrambled siRNA (“-“).

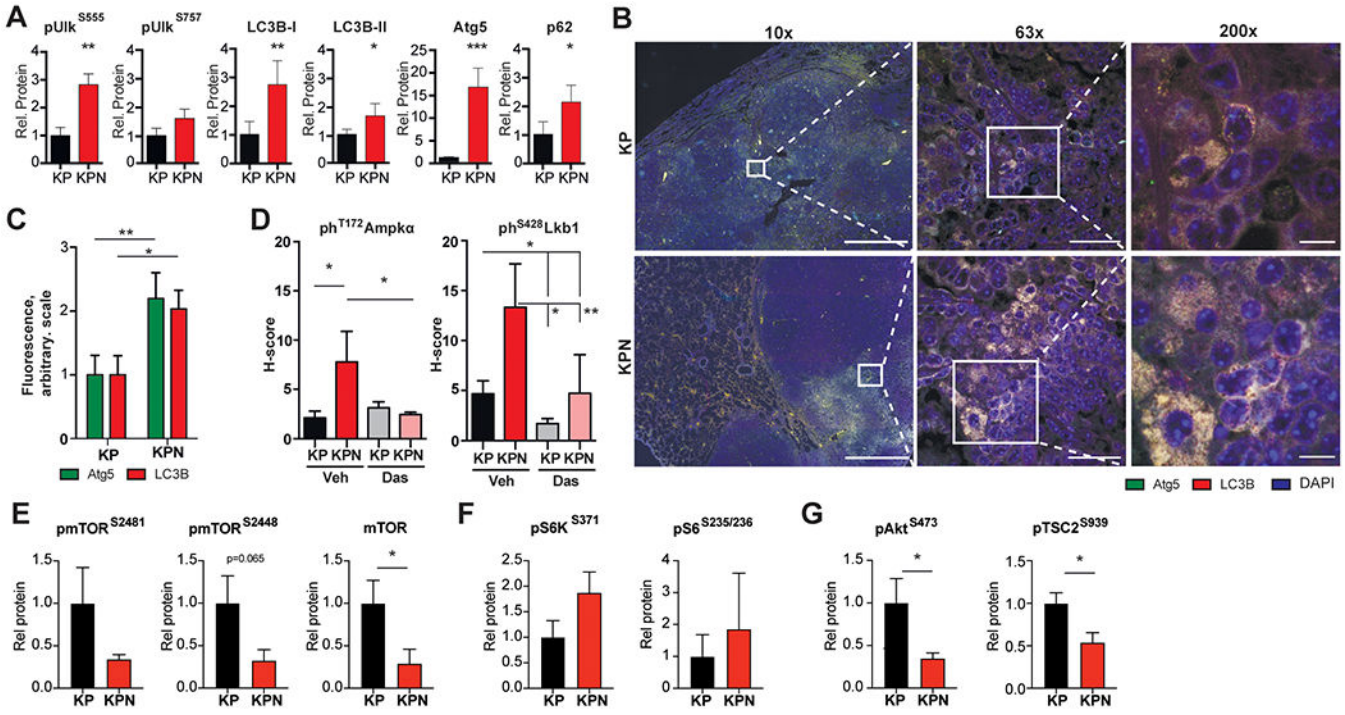

Figure 4. Autophagic signaling is elevated in KPN tumors.

A. Expression of indicated autophagic effector proteins quantified from Western blots of *KP* and *KPN* tumor lysates. **B.** Low (10x; scale bar 1 mm) and high magnification (63x; scale bar 45 μm and 200x; scale bar 10 um) images of lung tumors from *KP* and *KPN* mice, visualized by immunofluorescence, with antibodies to LC3B (red) and Atg5 (green). **C.** Integrated morphometry analysis-based quantitation of data from *KP* and *KPN* tumors as shown in **B**. **D.** Automated H-score quantitation of expression of ph^{S428}Lkb1 and ph^{T172}Ampk as visualized by immunohistochemical staining, in *KP* and *KPN* tumors, treated with vehicle or dasatinib. **E-G**. Expression and activation of mTOR (**E**), and phosphorylation of proteins conferred by mTORC1 (**F**) and mTORC2 (**G**), in KP and KPN tumor lysates. Statistics determined by Wilcoxon Rank-sum two-tailed tests; *, $p<0.05$, **, $p<0.01$, ***, $p<0.001$ versus control. All values shown for Western blot quantitations are normalized to Ponceau S staining of whole sample lane.

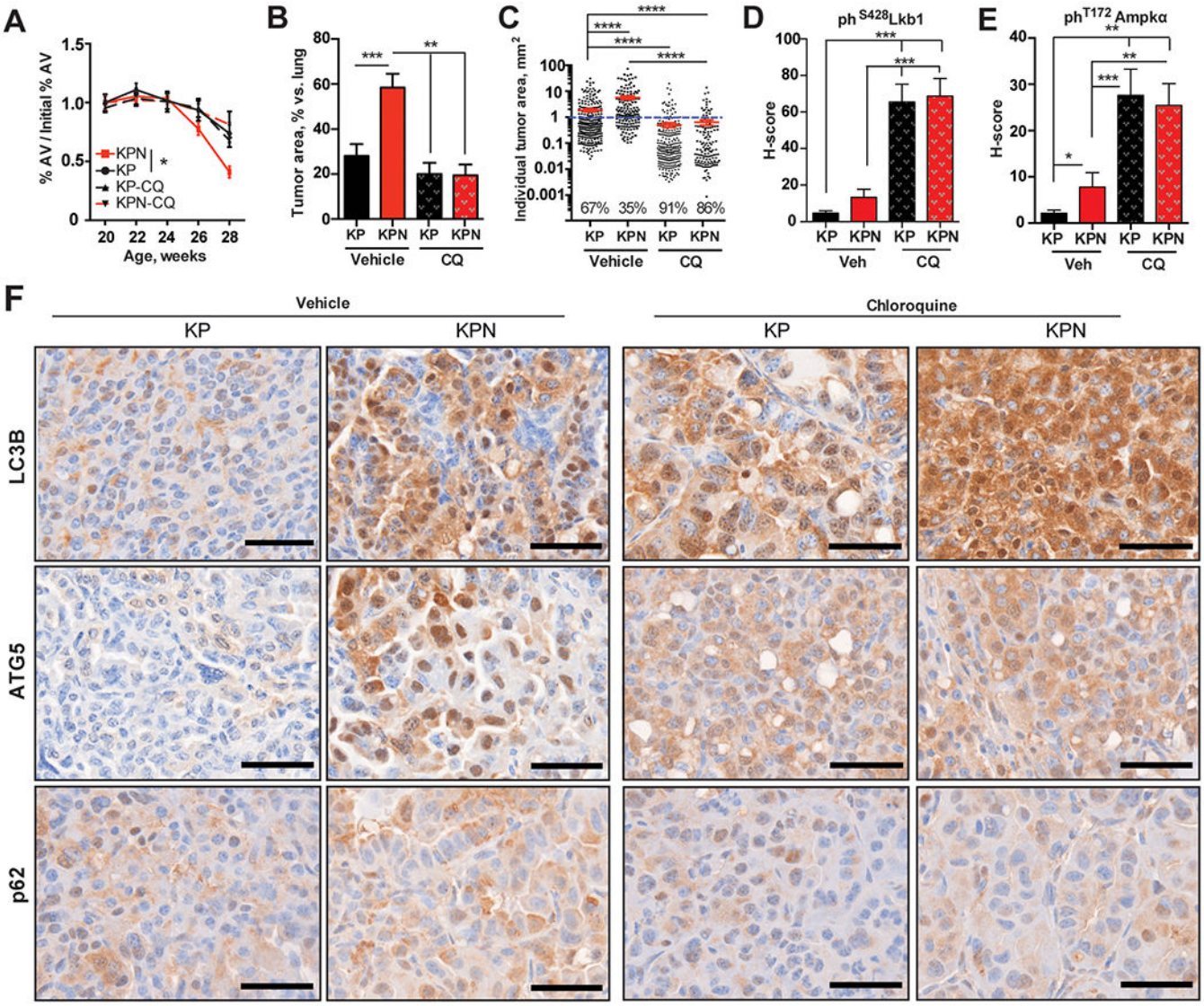

Figure 5. Inhibition of autophagy with chloroquine (CQ) eliminates elevated growth of KPN tumors.

A. Quantitation of tumor-induced reduction in lung airspace volume assessed by biweekly CT scanning of *KP* and *KPN* mice treated with vehicle or CQ. **B., C.** Total area (**B**) and size of individual tumors (% indicates tumors with area < 1mm^2) (**C**) in *KP* and *KPN* mice treated with vehicle or CQ. **D, E.** Automated H-score quantitation of expression of ph^{S428}Lkb1 (**D**) and ph^{T172}Ampα (**E**) as visualized by immunohistochemical staining, in *KP* and *KPN* tumors, treated with vehicle or CQ. **F.** Representative images of autophagosomes positive for LC3 (red) or Atg5 (green) in *KP* and *KPN* tumors treated with vehicle or CQ (40x; scale bar 45 μm). Statistics determined by Wilcoxon Rank-sum two-tailed tests; *, p<0.05, **, p<0.01, ***, p<0.001, ****, p<0.0001 for all graphs.